

Axial compressive behavior of concrete-filled steel tube columns with stiffeners

Wei Liang^{1,2a}, Jiangfeng Dong^{**1,3} and Qingyuan Wang^{*2,4}

¹ School of Architecture and Environment, Sichuan University, No. 24 South Section 1, Yihuan Road, Chengdu, 610065, China

² Key Laboratory of Deep Underground Science and Engineering, Ministry of Education, Sichuan University, Chengdu, 610065, China

³ Failure Mechanics and Engineering Disaster Prevention and Mitigation Key Laboratory of Sichuan Province, Sichuan University, Chengdu, 610065, China

⁴ State Key Laboratory of Hydraulics and Mountain River Engineering, Sichuan University, Chengdu, 610065, China

(Received November 29, 2017, Revised August 20, 2018, Accepted September 11, 2018)

Abstract. In order to reduce the deformation and delay the local buckling of concrete filled steel tube (CFST) columns, strengthening the structures with stiffeners is an effective method. In this paper, a new stiffening method with inclined stiffeners was used to investigate the behaviors of short CFST columns under axial compression. Besides, a three-dimensional nonlinear finite element (FE) model was applied to simulate the mechanical performances, including the total deformation, local buckling, and stress-strain relationship. Revised constitutive models of stiffened steel tube and confined concrete are proposed. A good agreement was achieved between the test and FE results. Furthermore, the calculated results of load capacity by using a simplified method also show a good correlation with experimental data.

Keywords: concrete filled steel tube (CFST) columns; self-compacting concrete (SCC); stiffening; axial compression; finite element analysis

1. Introduction

Due to the advantages such as high bearing capacity, high ductility and convenient construction, concrete-filled steel tube (CFST) columns are becoming increasingly applied in various structures in recent years. The composite action between the concrete and steel tube makes a great contribution to enhance the structural properties of CFST columns (Ren *et al.* 2014). The steel tube provides a confining pressure to the concrete to enhance the core's strength and ductility, while the core concrete prevents the steel tube from inward buckling (Chitawadagi *et al.* 2010, Elremaily and Azizinamini 2002). However, for the CFST columns with square or rectangular cross sections, the local outward buckling is easy to occur on the steel tube. This is due to the confinement is not strong enough (Dundu 2012, Aslani *et al.* 2015). In order to solve this problem and enhance the performance of CFST columns, there are four designations generally used in the CFST columns (Han *et al.* 2014): (1) concrete-filled double skin tubes (CFDST); (2) concrete-encased CFST; (3) CFST with additional reinforcement; (4) stiffened CFST. The experimental studies of stiffened CFST columns have shown that the local buckling of the steel tubes can be delayed effectively by the stiffened method, strengthening CFST columns with

stiffeners (Huang *et al.* 2002, Long and Cai 2013, Tao *et al.* 2005, Petrus *et al.* 2010). However, it is not easy to cast and vibrate the stiffened CFST columns to ensure the quality, because the layout of the tie bars or attached tab stiffeners complicate the structures. Therefore, self-compacting concrete (SCC) was applied in this experimental test. Self-compacting concrete is a special high-performance concrete that can flow under its own weight without segregation. Due to its excellent flowability and workability, SCC can flow through and fill the gaps of reinforcement and corners of molds without the need for additional mechanical vibration and compaction (Okamura and Ouchi 1998, Su *et al.* 2001). It makes SCC can be used for complicated constructions, heavy reinforced structures, or where the mechanical vibration is difficult. Moreover, since the industrial by-products such as fly ash, stone dust and silica fume can be used as filler materials in SCC, replacing some usage amount of cement with these by-products can lower the cost and environmental pollution (Topçu *et al.* 2009). Besides, the 28-day compressive strength values that ranged from 20 to 100 MPa were reported in the past researches (Domone 2006). This means that SCC with strengths may suit for most civil engineering situations with concrete.

In this paper, the steel tubes are strengthened with inclined stiffeners at the top, medium and bottom, the regions where the buckling occurs easily and two kinds of SCCs with different strengths were used to investigate the effect of concrete strength on CFST columns. The mechanical properties of these stiffened CFST columns under axial compression were tested and analyzed. Furthermore, a finite element model was developed to

*Corresponding author, Professor,
E-mail: wangqy@scu.edu.cn

**Associate Professor, E-mail: dongjf@scu.edu.cn

^a Ph.D. Student

simulate and predict the axial compressive resistances and the failure modes of stiffened CFST columns, and compared with experimental results.

2. Experimental program

In order to understand the basis of the numerical modeling method and assess the accuracy of the numerical simulations, the mechanical tests and experimental observations are summarized below.

2.1 Material properties

In order to investigate the effect of concrete strength on mechanical properties of CFST columns, two types of SCC were designed in this test. The results of fresh properties were tested by the slump flow test and U-box test. As the requirement of self-compacting concrete, the slump-flow diameter was suggested in the range of 550-700 mm and U-box filling height values should be in excess of 300 mm (Siddique 2013, Nepomuceno *et al.* 2014). Besides, the compressive cube strength of SCC at 28-day is recorded as f_{cu} . The flow properties and compressive strength of SCC are illustrated in Table 1, which has shown that the properties of fresh and hardened concrete were both deemed to satisfy the requirement. The properties of the steel are list as follow: the tensile strength is 390.0 MPa, the yield strength is 300.3 MPa, the elastic modulus is 195.4 GPa and the Poisson's ratio is 0.27.

2.2 Specimens and test setup

The design details of CFSTs are shown in Fig. 1 and

Table 1 Fresh properties and strength of SCC

Code	Slump-flow test		U-box test	f_{cu} (MPa)
	Dia.(mm)	T_{500} (s)	H (mm)	
SCC1	686	4.5	364	27.2
SCC2	631	3.4	323	56.3

Table 2 Properties and results of specimens

Specimen	n^*	w (mm)	f_{cu} (MPa)	α (%)	N_{ue} (kN)	DI
SCC1-F2W10	2	10	27.2	8.45	461	3.14
SCC1-F2W20	2	20	27.2	8.75	453	3.48
SCC1-F4W10	4	10	27.2	8.75	485	5.00
SCC1-F4W20	4	20	27.2	9.34	467	6.26
SCC2-F2W10	2	10	56.3	8.45	711	2.42
SCC2-F2W20	2	20	56.3	8.75	670	2.89
SCC2-F4W10	4	10	56.3	8.75	751	2.67
SCC2-F4W20	4	20	56.3	9.34	727	3.78

* n : Number of stiffened tube face; w : Width of stiffener; α : Steel ratio

Table 2. The width-to-thickness of the square tubes was set as 52 and the total length of the specimens was kept at 400 mm. The stiffeners were welded firmly on the inner wall of square steel tube by spot welding. Then the corresponding SCC was poured into the strengthened steel tube for casting the specimens. While the concrete initial setting, the end faces of specimens were covered with damp sponges to keep the concrete in the moist condition. After curing for 28 days, the moderate mortar was applied on the end faces of specimens, and then end faces were ground and polished to be flat and smooth after the mortar hardening. By this processing, the steel tube and inner concrete were expected to work together well and no concentrated force was applied on only one part of the specimen while suffering the axial load.

The test setup and instrument layout are shown in Fig. 2. All specimens were constructed and tested under axial compressive loads. Two linear variable displacement transducers (LVDTs) were set up between loading and bottom plates to measure the vertical displacement of the columns. To obtain the longitudinal and transverse strains of the specimens, six positions on the exterior of each CFST were selected to place the strain gauges. Two end plates with the thickness of 15 mm were placed between the test machine and specimen ends to avoid the end effect.

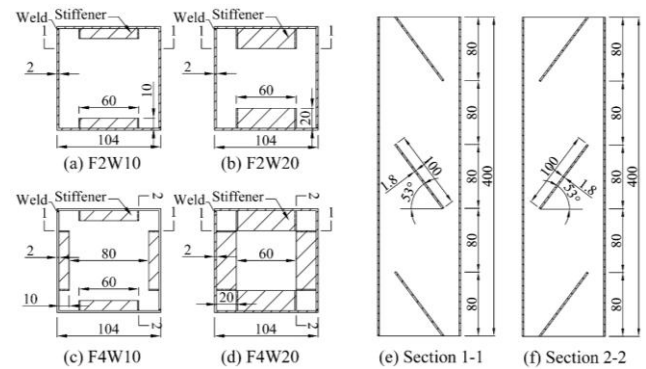


Fig. 1 Stiffening scheme

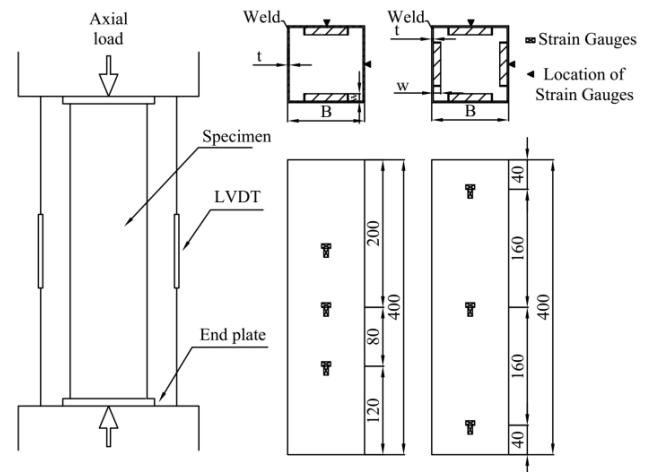


Fig. 2 Test setup and instrument layout

3. Experimental results and discussions

According to the experimental results, the load capacity, strain response and ductility of all specimens are presented in the following sections. The influence of the concrete strength and stiffening scheme on the properties of the CFST columns are also discussed and compared.

3.1 Load capacity

The experimental ultimate loads (N_{ue}) of the specimens under axial compression loading are listed in Table 2. The average load capacity of SCC2 specimens, which is 715 MPa, can be seen to be much higher than that of SCC1 specimens, which is 467 MPa. This is attributed to the higher compressive strength concrete in SCC2 specimens. However, the load capacities of specimens with the four stiffening schemes are very close. For SCC1 and SCC2 specimens, the standard deviation values are only 13.44 MPa and 34.06 MPa respectively. Moreover, the coefficients of variation have been calculated to be 2.88% and 4.77% respectively. This means that the effects of these stiffening schemes on the load capacities of CFST columns are not significant.

3.2 Strain response and ductility

The structural behavior of CFST columns can be described by the relationship between load and strain during

the loading process. The typical relationship can be generally characterized by the curve with three processes: the elastic stage, elastic-plastic stage and the post-peak stage (Chang *et al.* 2013). The tested load versus axial strain curves are shown in Fig. 3. It can be seen that all the columns performed in a similar way and the linear relationships approximately up to the 75-85% of the peak load respectively. By comparing the curves of series F2 and F4, specimens of F4 have a much smaller increase of axial strain than F2 specimens in the elastic stage and elastic-plastic stage. However, no noticeable difference could be found between the specimens with 10 mm and 20 mm stiffeners, especially in the elastic stage.

It is well-known that the ductility of CFST columns is mainly influenced by the factors, such as the axial compression ratio, the steel ratio, confining index and the strength of materials. As can be seen in Fig. 3, the declining trend of the load-axial strain curves of SCC1 specimens after the peak is slighter than that of SCC2 specimens. In order to quantify the effect of different stiffening schemes on ductility, the ductility index (DI) is adopted in this paper. It is expressed as (Tao *et al.* 2007)

$$DI = \frac{\varepsilon_{85\%}}{\varepsilon_y} \tag{1}$$

where, $\varepsilon_{85\%}$ is the nominal axial shortening (Δ / L) when the load falls to 85% of the ultimate load; $\varepsilon_y = \varepsilon_{75\%}/0.75$, and $\varepsilon_{75\%}$ is the nominal axial shortening when the load attains

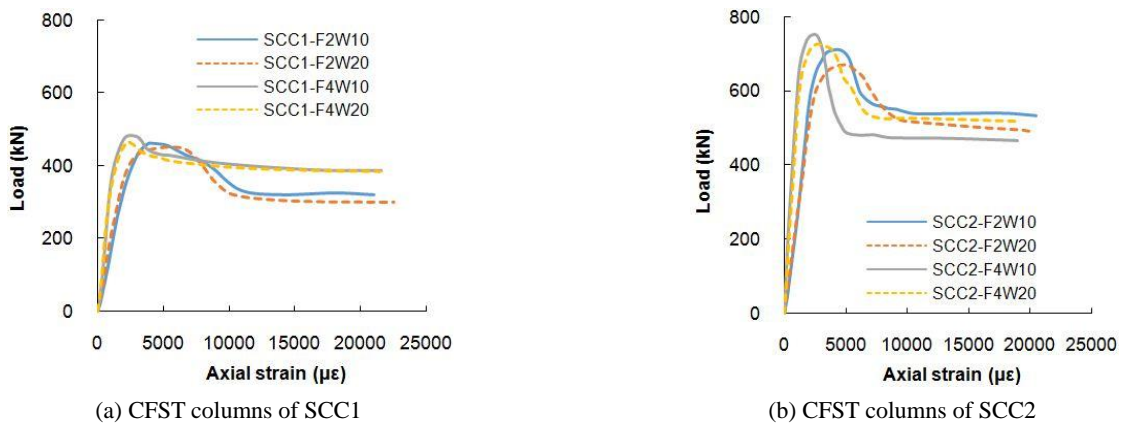


Fig. 3 Load-axial strain curves

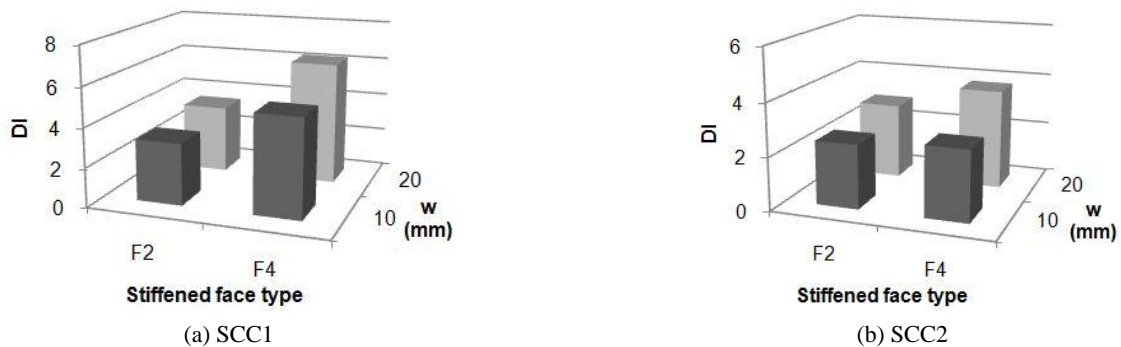


Fig.4 Effects of stiffeners on ductility

75% of the ultimate load in the pre-peak stage. The calculated ductility indexes are listed in Table 2. The effects of stiffeners on the ductility have been compared in Fig. 4. It can be seen that the specimens with SCC2 concrete have lower DI values, which means the worse ductility than that of SCC1 specimens. This is due to the fact that as the strength increases, the brittleness of concrete also increases and it may result in the sudden crack formation and unstable crack propagation (Gettu *et al.* 1990, Carpinteri 2012).

For both series of specimens filled with SCC1 and SCC2 concrete, the ductility indexes of F2W10 columns are the lowest and the F4W20 columns have the highest DI values. In general, the CFST columns with 20 mm stiffeners display better ductility than the ones with 10 mm stiffeners; and also, four-face stiffened CFST columns have better ductility than two-face stiffened ones.

4. Finite element analysis

ANSYS software was employed to perform numerical simulations of CFST columns that subjected to axial compression. The steel tube, stiffeners and concrete were modeled by using Solid 185, a 3D structural solid element. The element is defined by eight nodes and has the properties of plasticity, large deflection, large strain capabilities and so on for the nonlinear simulation to converge easily in processing. Fig. 5 shows the typical FE models for stiffened CFST columns.

Using an unreasonable element size would take a long time to solve the nonlinear problem and might get a non-convergent result. As suggested by Dai and Lam (2010), the concrete element size of 10 mm and steel element size of 5 mm was used in this FE model, and all the body parts of the model were meshed appropriately by hexahedron.

Two types of contacts are usually used for the interaction simulation of the steel tube and concrete: the interface bond and the surface-to-surface contact with an appropriate friction value. With bonded contacts, both

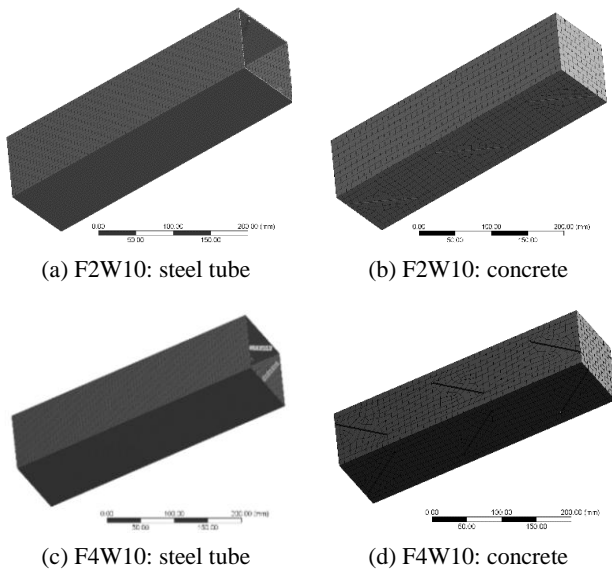


Fig. 5 Typical meshed FE model

surfaces are not allowed to separate and slide, they are bonded like glue. It was found that there were a negligible improvement and no obvious difference in the results by using the interface bond model (Bambach 2011). For CFST columns, the contact between the steel and concrete can be modeled with hard contact at a normal direction and Coulomb friction at the tangential direction (Tao *et al.* 2013). In the past, the friction coefficient was usually taken from 0.2 to 0.6. In the current FE model, the contacts between stiffeners and steel tube were defined as the bonded contacts, and the frictional contacts were used for the contact faces between the steel and concrete.

In order to compare the effect of different frictional coefficients, FE model for specimen SCC1-F2W10 was used as an example and frictional coefficients of 0.2, 0.4 and 0.6 were selected to investigate its effect on structural behavior. The results were shown in Fig. 6. It can be seen, there was very little difference. Therefore, the friction coefficient was taken as 0.4 in this paper. The Poisson's ratios for steel and concrete were taken as 0.27 and 0.3 respectively. Fixed boundary condition was applied to the bottom surface of the FE specimen, and axial loading was applied to the top surface by displacement control. To solve nonlinear equations, the full Newton-Raphson method with unsymmetric matrices was used in the analysis.

4.1 Stress-strain models of materials

To describe the constitutive relationship of steel, the stress-strain models are used in numerical analysis. For the cold-formed steel tube, an elastic-plastic constitutive model was suggested by Abdel-Rahman and Sivakumaran (Abdel-Rahman and Sivakumaran 1997). In this study, considering the steel tube was strengthened with stiffeners, a revised stress-strain curve based on multilinear isotropic strain hardening is proposed, as shown in Fig. 7. The expression is given as

$$\sigma = \begin{cases} E_s \varepsilon & , 0 \leq \varepsilon < \varepsilon_p \\ f_p + E_1 (\varepsilon - \varepsilon_p) & , \varepsilon_p \leq \varepsilon < \varepsilon_y \\ f_y + E_2 (\varepsilon - \varepsilon_y) & , \varepsilon_y \leq \varepsilon < \varepsilon_{st} \\ f_{st} + E_3 (\varepsilon - \varepsilon_{st}) & , \varepsilon \geq \varepsilon_{st} \end{cases} \quad (2)$$

where E_s is Young's modulus of elasticity, E_1 , E_2 and E_3 are slopes of lines, $E_1 = 0.25E_s$, $E_2 = 0.0025E_s$, $E_3 = 0.005E_s$; f_y is the yield strength; f_p and f_{st} are stress of feature points, f_p

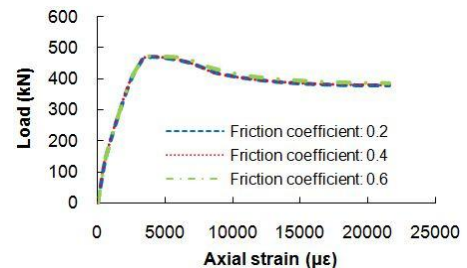


Fig. 6 The effect of friction coefficient on structural behavior

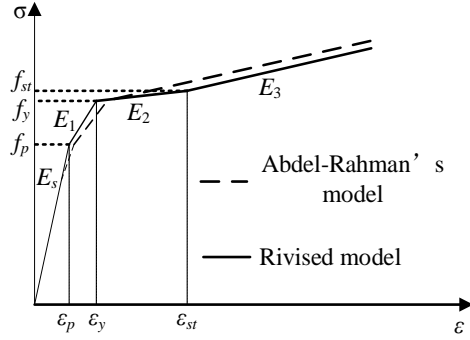


Fig. 7 Stress-strain model of stiffened steel tube

$= 0.85f_y, f_{st} = 1.05f_y$; $\varepsilon_p, \varepsilon_y$ and ε_{st} are strain of feature points, $\varepsilon_y = \varepsilon_p + 0.15f_y / E_1, \varepsilon_{st} = \varepsilon_y + 0.05f_y / E_2$.

It has been recognized that under compressive loading, steel tube can confine the lateral expanding of the core concrete, and increase its strength and ductility. The stress-strain relationships of confined concrete proposed by Han have been verified with a large amount of numerical test on CFST columns (Tao *et al.* 2009, Huang *et al.* 2010, Han *et al.* 2007). However, there is no special consideration for the confined concrete model for the CFST columns strengthened with stiffeners.

For CFST columns, the confinement can be affected by the contact interaction between the concrete and steel tube, including the section shape, wall thickness, constituent material properties and so on (Lam *et al.* 2012). In order to simulate the confined concrete for stiffened CFST columns, the stress-strain model based on Han's research was extended and applied in this paper. It is shown as following

$$y = \begin{cases} 2x - x^2, & (x \leq 1) \\ \frac{x}{\beta_0(x-1)^\eta + x}, & (x > 1) \end{cases} \quad (3)$$

where, $x = \varepsilon / \varepsilon_0$; $y = \sigma / \sigma_0$; σ_0 is the maximum stress of the confined concrete; ε_0 is the peak strain of the confined concrete; $\varepsilon_c = (1300 + 12.5\sigma_0) \times 10^{-6}$. For CFST with square section, $\eta = 1.6 + 1.5x, \beta_0 = \frac{\sigma_0^{0.1}}{1.2\sqrt{1+\xi}}$.

In this study, considering the stiffened steel tube has a great effect on the core concrete, the peak strain of the confined concrete based on regression analysis on the test data is given as

$$\sigma_0 = (-0.125c^2 + 0.6c + 0.1747)f_{cu} \quad (4)$$

where c is the influence coefficient of strengthening method on the peak strain, $c = n^{0.6}\xi^{0.1}$; n is the numbers of strengthened faces, as illustrated in Table 2.

And the peak strain can be expressed as

$$\varepsilon_0 = \left(\varepsilon_c + 800\xi^{0.2} \times 10^{-6} \right) \left[(1 + \xi)k_a^{0.6} + 1.8 \right] \left(\frac{1}{n} \right)^{0.6} \quad (5)$$

where k_a is the section influence coefficient, $k_a = 0.1e^a$; $a = A_{cor}/A_c$; A_{cor} is the effective core concrete area and it's

taken as the section area which excludes the projected area of stiffener and the area along the sides of stiffeners to the steel tube. In the above formula, the confinement factor for CFST columns and the expression is described as following

$$\xi = \frac{A_s f_y}{A_c f_{ck}} = \alpha \frac{f_y}{f_{ck}} \quad (6)$$

where A_s and A_c are the area of steel and concrete, α is the steel ratio and f_{ck} is the characteristic strength of concrete, equals to $0.67f_{cu}$ for normal strength concrete.

4.2 Validation of the finite element model

A comparison between the maximum axial compressive loads of experimental results (N_{ue}) and numerical predictions (N_{FE}) is illustrated in Table 3. As can be seen, the numerical results of FE models are in good agreement with experiments. Even the N_{FE} values of SCC1 are a little larger and N_{FE} values of SCC2 are smaller than the corresponding experimental results, the maximum difference is only 4%. The curves of load versus axial strain of FE models are plotted against the experimental data in Fig. 8. It can be seen that the simulated curve is basically consistent with the test curve before the load reaches the ultimate compressive bearing capacity of the specimen. This indicates that the FE model can well simulate the mechanical performance of the specimen under axial load, especially the specimen is in the elastic stage and elastic-plastic stage. However, the simulated strain value at the post-peak stage is much higher than the tested strain, and the declining trend of the simulated load-strain curve is very slight. This is due to that the finite element calculation is very difficult after the defined concrete element reaches its failure criterion, although the stress-strain relation of concrete after failure is taken into the FE model.

The specimens, SCC1-F2W10, SCC1-F4W10 and SCC2-F4W10, are used as examples to show the typical deformation and stress distribution of CFST columns with inclined stiffeners, as shown in Fig. 9. The total deformation of FE models is similar to that observed from experiments: the local buckling often appears at the top, the bottom or near the middle. As can be seen clearly in

Table 3 Comparison of maximum loads from experimental and calculation results

Specimen	N_{ue} (kN)	N_{FE} (kN)	N_c (kN)	N_{FE}/N_{ue}	N_c/N_{ue}
SCC1-F2W10	461	472	447	1.02	0.97
SCC1-F2W20	453	464	430	1.02	0.95
SCC1-F4W10	485	490	532	1.01	1.10
SCC1-F4W20	467	486	500	1.04	1.07
SCC2-F2W10	711	708	761	1.00	1.07
SCC2-F2W20	670	653	744	0.97	1.11
SCC2-F4W10	751	730	856	0.97	1.13
SCC2-F4W20	727	717	813	0.99	1.12

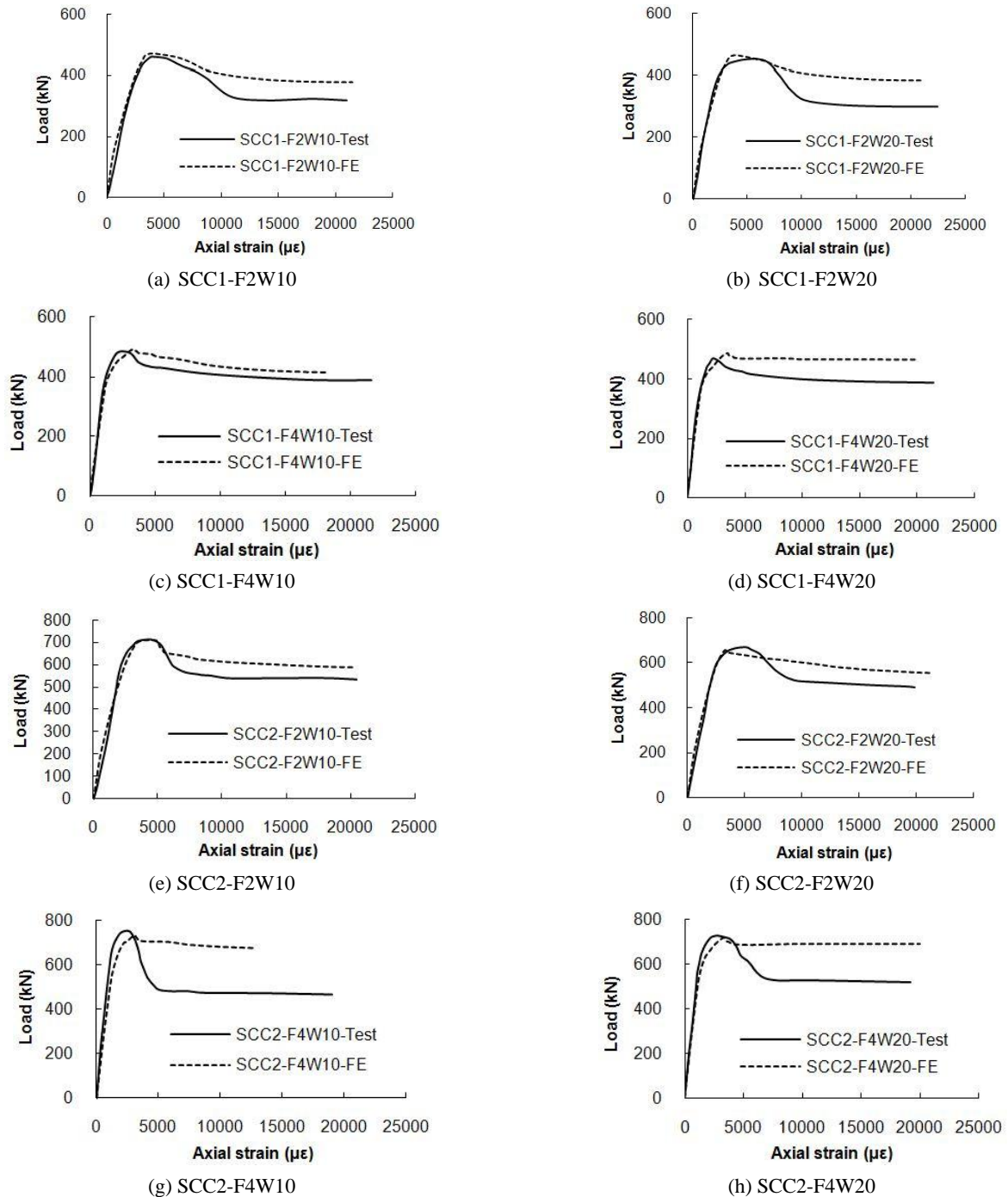


Fig.8 Comparison of experimental and numerical results for CFST columns with inclined stiffeners

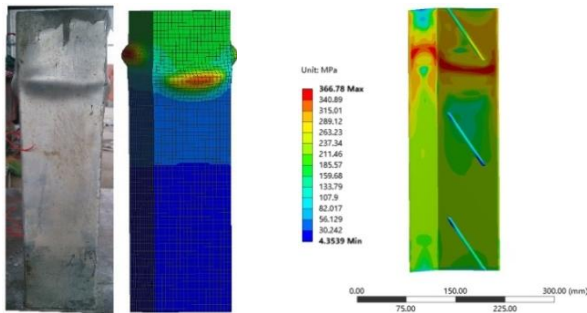
Figs. 9(b), (d) and (f), the maximum stress of steel tube is found at the ends of stiffeners, the region without stiffening. As shown in Fig. 9(b), the maximum stress region at the unstiffened face is closer to the top than that at stiffened face. Moreover, for the four-face stiffened CFST columns, the maximum stress regions appear at nearly the same horizontal plane and are all close to the ends of stiffeners.

4.3 Stress analysis

In order to compare and analyze the interaction between steel tube, stiffeners and concrete, the specimen SCC1-

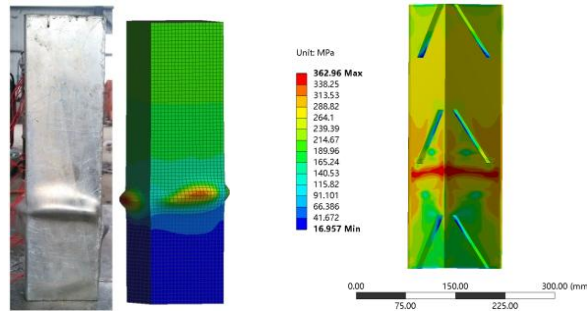
F2W10 is taken as an example and the stress distributions of multiple characteristic locations on this specimen, including the longitudinal middle line of the stiffened and unstiffened faces of steel tube (Line 1 and Line 2), the middle section of the interval area of the oblique stiffeners (Section A), the middle section of the specimen (Section B) and the section of the end of the stiffeners (Section C), are selected as shown in Fig. 10.

The stress changes along Line 1 and Line 2 on steel tube are shown in Fig. 11. It can be seen that before the axial load reaches the ultimate bearing capacity of the specimen, the maximum transversal stress appears at the range 55~75



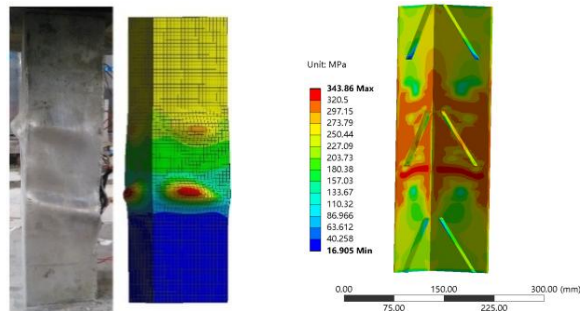
(a) Total deformation of SCC1-F2W10

(b) Stress distribution of SCC1-F2W10 steel tube (Diagonal section view)



(c) Total deformation of SCC1-F4W10

(d) Stress distribution of SCC1-F4W10 steel tube (Diagonal section view)



(e) Total deformation of SCC2-F4W10

(f) Stress distribution of SCC2-F4W10 steel tube (Diagonal section view)

Fig. 9 Typical deformation and stress distribution of CFST columns with inclined stiffeners

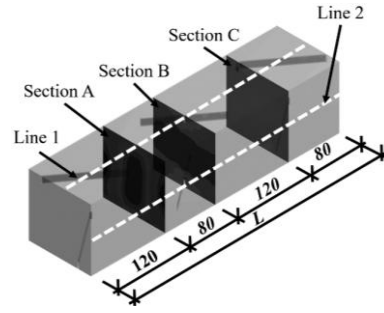
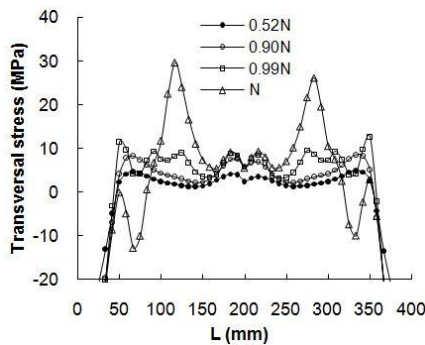


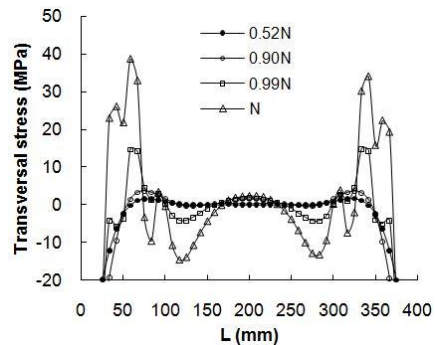
Fig. 10 The extracted path of stress

mm from the end face of the specimen. Besides, with the increase of load, the transversal stress on the unstiffened face has no obvious change, and the transversal stress on stiffened face grows gradually. This is due to that the stiffeners are bonded with steel tube firmly, the force generated by concrete deformation on stiffeners also works on steel tube and lead to that the stiffened wall of steel tube suffers larger transversal stress. When the ultimate load is reached, the local buckling on stiffened face appears within the interval range of the stiffeners, where has approximately 120 mm from the end face of the specimen. Besides, the local buckling on unstiffened face appears at the position that gets about 60 mm from the end face, and it is basically consistent with the position of maximum transversal stress. The result indicates that setting of stiffeners significantly changes the position of local buckling and also has constraint effect on the deformation at the corresponding position on steel tube.

The longitudinal stress of concrete in three different section is shown in Fig. 12. As can be seen, the maximum stress of concrete at Section A occurs close to both unstiffened sides, while the position of the minimum stress is near the stiffened sides. At Section B, the compressive stress at the stiffened sides is minimum, while the maximum stress occurs at the end of stiffeners, and the range of the maximum stress gradually expands to the middle of Section B with the increasing load. At Section C, the stress of concrete near the longitudinal end of the stiffener is obviously greater than that of the concrete near to both sides of the stiffener. In addition, compared with the stress of Section B and Section C, the average stress of



(a) Line 1



(b) Line 2

Fig. 11 The transversal stress on the stiffened and unstiffened faces of steel tube

Section A is larger when the same load is applied on the specimen, and the difference between maximum and minimum stress is much small. It can be noticed that the stress difference is larger in the section with stiffeners and the failure of concrete begins at the position of the stress concentration.

5. Simplified method of load capacity prediction

For stiffened CFST columns, the load of the composite section can be expressed as (Tao *et al.* 2005)

$$N_p = A_{sc} f_{scy} + A_{ss} f_{ys} \quad (7)$$

where A_{sc} is the sum of cross-sectional areas of the steel tube and the concrete core, f_{scy} is the nominal average strength of a square or rectangular steel tube after filling with concrete; A_{ss} is the area of the section of stiffener; and f_{ys} is the yield strength of stiffener.

In this paper, the load capacity of stiffened CFST column is expressed as

$$N_c = r(A_{sc} f_{scy}^s + A_{ss} f_{ys}) \quad (8)$$

where r is the reduction factor, considering the effect of initial imperfections of structures and the weakness of welded lines of steel tube, $r = 0.85$; f_{scy}^s is the nominal average strength of stiffened steel tube after filling with concrete, $f_{scy}^s = (1.15 + 2.85k_c)f_{ck}$; k_c is the coefficient of axial compression strength for stiffened CFST column, which takes the effects of confinement factor, stiffened scheme and effective concrete core into account

$$k_c = \xi k_n k_a \quad (9)$$

where k_n is the influence coefficient of stiffened faces, $k_n = 0.57n^{0.8}$; k_a is taken the same as explained in Eq. (5).

The calculation results (N_c) are listed in Table 3. The average value of N_c/N_{ue} is 1.065 and standard deviation is 0.07. It can be seen that the calculation results agree well with test data.

6. Conclusions

This paper presents the nonlinear analysis of CFST columns with inclined stiffeners under axial compression. Considering the effects of the strengthening method on strength and sections of columns, revised stress-strain models for steel tube and confined concrete are proposed respectively. The following conclusions can be drawn based on the experimental results of the study:

- Setting stiffeners on the steel tube of CFST can delay the occurrence of local buckling and suppress the deformation degree of local buckling after the ultimate bearing capacity is reached. And the ductility of four-face stiffened columns is much better than that of two-face stiffened ones.

- Different stiffening schemes in this paper have no significant effect on the ultimate bearing capacity of the specimen. For the specimens in series SCC1 and SCC2, the standard deviation values are only 13.44 MPa and 34.06 MPa respectively. This is due to the fact that the effective working areas of the sections of different specimens are basically the same. And the failure of inner concrete begins from the positions that near to the ends of stiffeners.
- The modified stress-strain model of steel and concrete are established and applied in the finite element (FE) models of stiffened CFST. The simulated results can reflect the mechanical performances of tested specimens well, including the total deformed shape, the local buckling region, the load-deformation response and the ultimate bearing capacity. Besides, the working mechanism of CFST columns with stiffeners under axial loading is analyzed with the FE model.
- Considering the effect of stiffeners, a simple calculation model for predicting the ultimate bearing capacity of stiffened CFST under axial compressive load is established. The average ratio of calculated value to the tested value is 1.065. It shows that the calculated results are in good agreement with the experimental results.

Acknowledgments

The authors are grateful for the financial support towards this research provided by the National Natural Science Foundation of China (No. 51408382).

References

- Abdel-Rahman, N. and Sivakumaran, K.S. (1997), "Material properties models for analysis of cold-formed steel members", *J. Struct. Eng.*, **123**(9), 1135-1143.
- Aslani, F., Uy, B., Tao, Z. and Mashiri, F. (2015), "Predicting the axial load capacity of high-strength concrete filled steel tubular columns", *Steel Compos. Struct., Int. J.*, **19**(4), 967-993.
- Bambach, M.R. (2011), "Design of hollow and concrete filled steel and stainless steel tubular columns for transverse impact loads", *Thin Wall. Struct.*, **49**(10), 1251-1260.
- Carpinteri, A. (2012), *Mechanical Damage and Crack Growth in Concrete: Plastic Collapse to Brittle Fracture*, Springer Science & Business Media.
- Chang, X., Fu, L., Zhao, H.-B. and Zhang, Y.-B. (2013), "Behaviors of axially loaded circular concrete-filled steel tube (CFT) stub columns with notch in steel tubes", *Thin Wall. Struct.*, **73**, 273-280.
- Chitawadagi, M.V., Narasimhan, M.C. and Kulkarni, S.M. (2010), "Axial strength of circular concrete-filled steel tube columns — DOE approach", *J. Constr. Steel Res.*, **66**(10), 1248-1260.
- Dai, X. and Lam, D. (2010), "Numerical modelling of the axial compressive behaviour of short concrete-filled elliptical steel columns", *J. Constr. Steel Res.*, **66**(7), 931-942.
- Domone, P.L. (2006), "Self-compacting concrete: An analysis of 11 years of case studies", *Cem. Concrete Compos.*, **28**(2), 197-208.
- Dundu, M. (2012), "Compressive strength of circular concrete filled steel tube columns", *Thin Wall. Struct.*, **56**, 62-70.

- Elremaily, A. and Azizinamini, A. (2002), "Behavior and strength of circular concrete-filled tube columns", *J. Constr. Steel Res.*, **58**, 1567-1591.
- Gettu, R., Bazant, Z.P. and Karr, M.E. (1990), "Fracture properties and brittleness of high-strength concrete", *ACI Mater. J.*, **87**(6), 608-618.
- Han, L.-H., Yao, G.-H. and Tao, Z. (2007), "Performance of concrete-filled thin-walled steel tubes under pure torsion", *Thin Wall. Struct.*, **45**(1), 24-36.
- Han, L.-H., Li, W. and BJORHOVDE, R. (2014), "Developments and advanced applications of concrete-filled steel tubular (CFST) structures: Members", *J. Constr. Steel Res.*, **100**, 211-228.
- Huang, C. S., Yeh, Y.-K., Liu, G.-Y., Hu, H.-T., Tsai, K.C., Weng, Y.T., Wang, S.H. and Wu, M.-H. (2002), "Axial Load Behavior of Stiffened Concrete-Filled Steel Columns", *J. Struct. Eng.*, **128**(9), 1222-1230.
- Huang, H., Han, L.-H., Tao, Z. and Zhao, X.-L. (2010), "Analytical behaviour of concrete-filled double skin steel tubular (CFDST) stub columns", *J. Constr. Steel Res.*, **66**(4), 542-555.
- Lam, D., Dai, X.H., Han, L.H., Ren, Q.X. and Li, W. (2012), "Behaviour of inclined, tapered and STS square CFST stub columns subjected to axial load", *Thin Wall. Struct.*, **54**, 94-105.
- Long, Y.-L. and Cai, J. (2013), "Stress-strain relationship of concrete confined by rectangular steel tubes with binding bars", *J. Constr. Steel Res.*, **88**, 1-14.
- Nepomuceno, M.C.S., Pereira-de-Oliveira, L.A. and Lopes, S.M.R. (2014), "Methodology for the mix design of self-compacting concrete using different mineral additions in binary blends of powders", *Constr. Build. Mater.*, **64**, 82-94.
- Okamura, H. and Ouchi, M. (1998), "Self-compacting high performance concrete", *Progress in Structural Engineering and Materials*, **1**(4), 378-383.
- Petrus, C., Abdul Hamid, H., Ibrahim, A. and Parke, G. (2010), "Experimental behaviour of concrete filled thin walled steel tubes with tab stiffeners", *J. Constr. Steel Res.*, **66**(7), 915-922.
- Ren, Q.X., Hou, C., Lam, D. and Han, L.H. (2014), "Experiments on the bearing capacity of tapered concrete filled double skin steel tubular (CFDST) stub columns", *Steel Compos. Struct., Int. J.*, **17**(5), 667-686.
- Siddique, R. (2013), "Compressive strength, water absorption, sorptivity, abrasion resistance and permeability of self-compacting concrete containing coal bottom ash", *Constr. Build. Mater.*, **47**, 1444-1450.
- Su, N., Hsu, K.-C. and Chai, H.-W. (2001), "A simple mix design method for self-compacting concrete", *Cem. Concrete Res.*, **31**, 1799-1807.
- Tao, Z., Han, L.-H. and Wang, Z.-B. (2005), "Experimental behaviour of stiffened concrete-filled thin-walled hollow steel structural (HSS) stub columns", *J. Constr. Steel Res.*, **61**(7), 962-983.
- Tao, Z., Han, L.-H. and Wang, D.-Y. (2007), "Experimental behaviour of concrete-filled stiffened thin-walled steel tubular columns", *Thin Wall. Struct.*, **45**(5), 517-527.
- Tao, Z., Uy, B., Han, L.-H. and Wang, Z.-B. (2009), "Analysis and design of concrete-filled stiffened thin-walled steel tubular columns under axial compression", *Thin Wall. Struct.*, **47**(12), 1544-1556.
- Tao, Z., Wang, Z.-B. and Yu, Q. (2013), "Finite element modelling of concrete-filled steel stub columns under axial compression", *J. Constr. Steel Res.*, **89**, 121-131.
- Topçu, İ.B., Bilir, T. and Uygunoğlu, T. (2009), "Effect of waste marble dust content as filler on properties of self-compacting concrete", *Constr. Build. Mater.*, **23**(5), 1947-1953.